Giant vortices in combined harmonic and quartic traps

Amandine Aftalion* and Ionut Danaila†
Laboratoire Jacques-Louis Lions, Université Paris 6, 175 rue du Chevaleret, 75013 Paris, France
(Received 29 September 2003; revised manuscript received 11 December 2003; published 18 March 2004)

We consider a rotating Bose-Einstein condensate confined in combined harmonic and quartic traps, following recent experiments [V. Bretin, S. Stock, Y. Seurin, and J. Dalibard, Phys. Rev. Lett. **92**, 050403 (2004)]. We investigate numerically the behavior of the wave function which solves the three-dimensional Gross Pitaevskii equation and analyze in detail the structure of vortices. For a quartic-plus-harmonic potential, as the angular velocity increases, the vortex lattice evolves into a vortex array with hole. The merging of vortices into the hole is highly three dimensional, starting from the top and bottom of the condensate to reach the center. We also investigate the case of a quartic-minus-harmonic potential, not covered by experiments or previous numerical works. For intermediate repulsive potentials, we show that the transition to a vortex array with hole takes place for lower angular velocities, when the lattice is made up of a small number of vortices. For the strong repulsive case, a transition from a giant vortex to a hole with a circle of vortices around is observed.

DOI: 10.1103/PhysRevA.69.033608 PACS number(s): 03.75.−b, 02.70.−c

I. INTRODUCTION

The existence and formation of quantized vortices have recently been widely studied in Bose-Einstein condensates [1–7]. One type of experiments consists in rotating the magnetic trap confining the atoms. For a harmonic trapping potential, and a rotating frequency Ω close to $0.7\omega_\perp$, which is the transverse trapping frequency, vortices start to appear and arrange themselves into a lattice [5]. As Ω is increased, the number of vortices increases as well and the lattice gets denser. As Ω reaches $\omega_\perp$, the confinement vanishes since the centrifugal force compensates the trapping force. This regime is the focus of a lot of attention since new physical phenomena are expected for these fast rotating gases.

Using stiffer trapping potentials than the harmonic one, allows to explore the regime $\Omega > \omega_\perp$. Theoretical and numerical studies have considered trapping potentials behaving like r^n or r^2+r^4 [8–12]. A rich variety of vortex states is predicted: lattice of singly quantized vortices, array of vortices with a hole in the center, and giant (multiple quantized) vortices. This type of trapping, which eliminates the singular behavior at $\Omega=\omega_\perp$, has recently been achieved experimentally by superimposing a blue detuned laser beam to the magnetic trap holding the atoms [13,14]. The resulting potential is

$$V_{trap}(r,z) = V_h(r,z) + U(r), \tag{1}$$

with

$$V_h = \frac{1}{2}m\omega_\perp^2 r^2 + \frac{1}{2}m\omega_z^2 z^2 \quad \text{and } U(r) = U_0 \exp\left(-\frac{2r^2}{w^2}\right). \tag{2}$$

For r/w sufficiently small, the resulting potential can be approximated by

$$V_{trap} \simeq \left[\frac{1}{2}m\omega_\perp^2 - \frac{2U_0}{w^2}\right]r^2 + \frac{2U_0}{w^4}r^4 + \frac{1}{2}m\omega_z^2 z^2. \tag{3}$$

In experiments, the amplitude U_0 of the superimposed laser is small, so that the coefficient of the r^2 term is positive.

In this paper, we investigate the three-dimensional structure of stable states (vortex lattice, vortex array with hole, giant vortices) of the condensate in the framework of the Gross Pitaveskii energy. First, we study the three-dimensional vortices for the *quartic-plus-harmonic* trapping potential (3) corresponding to the experiments [14]. This contributes not only to complete the simplified two-dimensional (2D) picture given by previous studies but also to remove some of the questions concerning the 3D effects (such as vortex bending) in the experimental observations of Refs. [13,14]. Second, if the amplitude U_0 of the laser is increased to change the sign of the harmonic part of the potential (3), i.e.,

$$\frac{1}{2}m\omega_\perp^2 < \frac{2U_0}{w^2}, \tag{4}$$

we show that such a *quartic-minus-harmonic* trapping potential allows to obtain vortex arrays with hole and giant vortices for lower Ω than obtained previously. The difference in lowering the frequency Ω of nucleation of the giant vortex is that this vortex structure does not appear as a consequence of a very dense lattice but due to a small number of vortices merging together. The three-dimensional structure of the merging is analyzed. This leads to new open problems in terms of theoretical studies.

Finally, we study the case of a strong repulsive potential which acts like a pinning potential at low velocity. Nevertheless, when Ω is increased, the giant vortex turns into a giant vortex with a circle of singly quantized vortices around.

II. NUMERICAL APPROACH

We consider a pure BEC of N atoms confined in a trapping potential V_{trap}, rotating along the z axis at angular ve-

*Electronic address: aftalion@ann.jussieu.fr
†Electronic address: danaila@ann.jussieu.fr

locity Ω. The equilibrium of the system corresponds to local minima of the Gross-Pitaevskii energy in the rotating frame

$$\mathcal{E}(\phi) = \int_{\mathcal{D}} \frac{\hbar^2}{2m}|\nabla\phi|^2 + \hbar\boldsymbol{\Omega}\cdot(i\phi, \nabla\phi\times\mathbf{x}) + V_{trap}|\phi|^2 + \frac{N}{2}g_{3D}|\phi|^4, \quad (5)$$

where $g_{3D}=4\pi\hbar^2 a/m$ and the wave function ϕ is normalized to unity $\int_{\mathcal{D}}|\phi|^2=1$.

For numerical purposes, it is convenient to rescale the variables as follows: $\mathbf{r}=\mathbf{x}/R$, $u(\mathbf{r})=R^{3/2}\phi(\mathbf{x})$, where $R=d/\sqrt{\varepsilon}$ and

$$d=\left(\frac{\hbar}{m\omega_\perp}\right)^{1/2}, \quad \varepsilon=\left(\frac{d}{8\pi Na}\right)^{2/5}, \quad \tilde{\Omega}=\Omega/(\varepsilon\omega_\perp). \quad (6)$$

In this scaling, the trapping potential (3) becomes

$$V(\mathbf{r}) = (1-\alpha)r^2 + \frac{1}{4}kr^4 + \beta^2 z^2, \quad (7)$$

where

$$\alpha=\frac{4U_0}{m\omega_\perp^2 w^2}, \quad k=4\alpha\left(\frac{R}{w}\right)^2, \quad \beta=\frac{\omega_z}{\omega_\perp}. \quad (8)$$

Note that we take $\omega_\perp$ (which is the frequency of the original harmonic potential V_h) as a scaling frequency for Ω, and not the effective harmonic trapping frequency $\omega_\perp^{(e)}=\omega_\perp\sqrt{|1-\alpha|}$, as in Ref. [13]. For numerical applications, we choose $\varepsilon=0.02$, $\beta=\omega_z/\omega_\perp=1/7$, $k/\alpha=0.25$, which fit the experimental values [13]. In Ref. [13], $\alpha=0.25$, but we will take bigger values since our aim is to understand the influence of α when it gets bigger than 1 and changes the sign of the harmonic part.

Then, we use the dimensionless energy introduced in Ref. [15],

$$E(u) = H(u) - \tilde{\Omega}L_z(u), \quad (9)$$

where H is the Hamiltonian,

$$H(u) = \int \frac{1}{2}|\nabla u|^2 + \frac{1}{2\varepsilon^2}V(\mathbf{r})|u|^2 + \frac{1}{4\varepsilon^2}|u|^4, \quad (10)$$

and L_z the angular momentum axis

$$L_z(u) = i\int \bar{u}\left(y\frac{\partial u}{\partial x} - x\frac{\partial u}{\partial y}\right). \quad (11)$$

Using a hybrid Runge-Kutta-Crank-Nicolson scheme described in Ref. [15], we compute critical points of $E(u)$ by solving the norm-preserving imaginary time propagation of the corresponding equation

$$\frac{\partial u}{\partial t} - \frac{1}{2}\nabla^2 u + i(\tilde{\boldsymbol{\Omega}}\times\mathbf{r})\cdot\nabla u = -\frac{1}{2\varepsilon^2}u(V+|u|^2) + \mu_\varepsilon u, \quad (12)$$

where μ_ε is the Lagrange multiplier for the constraint $\int_{\mathcal{D}}|u|^2=1$ and with $u=0$ on $\partial\mathcal{D}$. Here, $\mathcal{D}$ is a rectangular domain containing the condensate. A typical simulation uses a domain $(x,y,z)\in[-2,2]\times[-2,2]\times[-2.8,2.8]$ with a refined grid of $200\times200\times140$ nodes, which is sufficient to achieve grid independence for all considered numerical experiments.

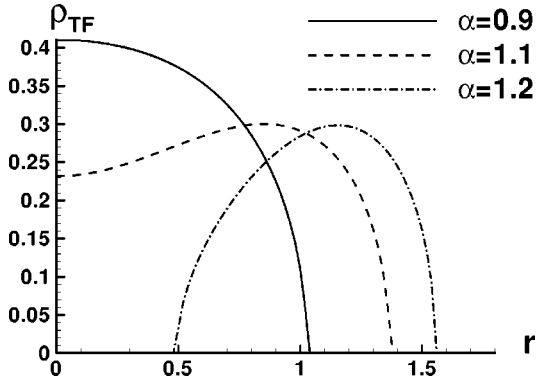

FIG. 1. Thomas-Fermi limit ρ_{TF} for different values of α.

We first compute the steady-state corresponding to a nonrotating ($\Omega=0$) condensate, using as initial condition $u=\sqrt{\rho_{\mathrm{TF}}}$, the Thomas-Fermi profile

$$\rho_{\mathrm{TF}}(\mathbf{r}) = \rho_0 - V(\mathbf{r}) = \rho_0 + (\alpha-1)r^2 - \frac{1}{4}kr^4 - \beta^2 z^2. \quad (13)$$

Depending on the choice of α, the Thomas-Fermi density profile can display three different shapes, as shown in Fig. 1. The corresponding steady solutions obtained for $\Omega=0$ (which will be used as initial conditions for the subsequent runs with $\Omega>0$) are displayed in Fig. 2. We can distinguish three cases.

(i) $\alpha<1$ (weak attractive case) is the case closest to the experiments and is strongly influenced by the (positive) harmonic part. For $\Omega=0$, a classical prolate condensate is obtained. As Ω increases, the effective trapping potential $V^{eff}(\mathbf{r})=V(\mathbf{r})-\varepsilon^2\Omega^2 r^2$ starts to have a Mexican hat structure. A vortex lattice appears for intermediate values of Ω and turns into a lattice with a hole for large Ω.

(ii) $1<\alpha<1+\xi$, with $\xi=\beta^{1/4}k^{5/8}/\sqrt{\pi}$ (intermediate repulsive case): at $\Omega=0$, as an imprint of the negative harmonic part, the density profile has a depletion close to the center but

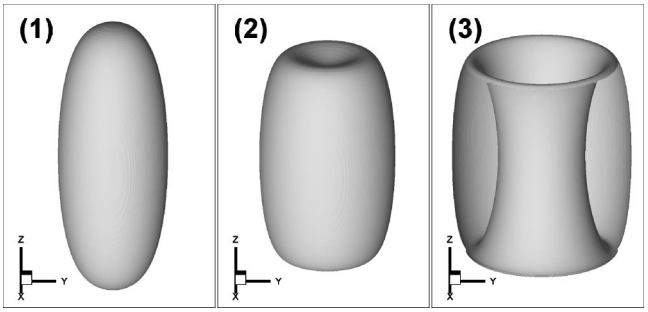

FIG. 2. Different shapes of the condensate at $\Omega=0$: isosurfaces of lowest density in the condensate for $\alpha=0.9$ (picture 1), 1.1 (picture 2), 1.2 (picture 3).

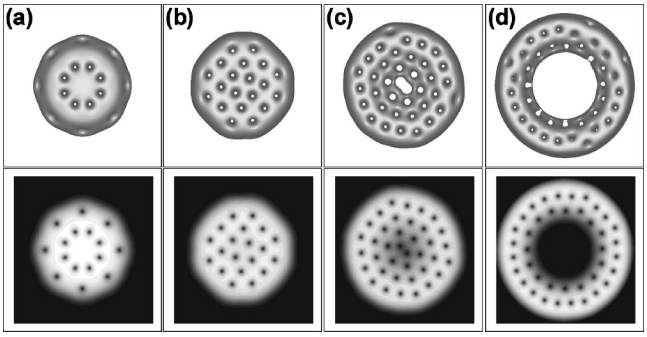

FIG. 3. ($\alpha=0.9$) Top view of the isosurface of lowest density (up) and density contours in the plane $z=0$ (down) for $\Omega/\omega_\perp=0.32$ (a), 0.4 (b), 0.48 (c), and 0.56 (d).

no hole. The density profile starts to have a hole for intermediate values of Ω.

(iii) $\alpha>1+\xi$ (strong repulsive case): the density profile has a hole for all Ω.

III. DESCRIPTION OF THE RESULTS

We show the three-dimensional structure of vortices in details. The first two cases (weak attractive and intermediate repulsive) display a similar transition from a vortex lattice to an array of vortices with a central hole when Ω is increased and the merging process starts from the top and bottom of the condensate to reach the center. This is due to the fact that as Ω is increased, the effective potential has a Mexican hat structure. The difference though is that for the intermediate repulsive case, the phenomenon does not take place at high rotation value. The vortex lattice is not so dense.

In the last case (strong repulsive), giant vortices are obtained for low Ω and a hole with a circle of vortices around for larger Ω, that is the transition takes place in the opposite direction.

A. Weak attractive case ($\alpha=0.9$)

This is the case closest to the experiments [13,14].The density profile of the solutions are shown in Figs. 3 (top view and 2D cut in the plane $z=0$) and 4 (three-dimensional structure).

At low Ω [Figs. 3, 4(a), and 4(b)], there are isolated singly quantized vortices, forming a lattice. As Ω is increased, the vortex lattice gets denser [20 vortices in Fig. 3(b) and 38 in Fig. 3(c)]. As a consequence, the angular momentum L_z grows rapidly to high values (Fig. 5). It is interesting to note from the side view of the condensate (Fig. 4) that most vortices of the lattice are straight but some are bending. This explains why the values of L_z in Fig. 5 are slightly lower than the corresponding number of vortices.

As Ω is further increased ($\Omega/\omega_\perp=0.48$), a hole starts to appear at the center of the condensate [Fig. 3(c)]. It is clear from Figs. 3(c) and 4(c) that close to $z=0$, the lattice has not merged into a hole, while close to the top, there is already a giant vortex. This phenomenon is highly three dimensional. However, this central depletion is not strong enough to explain alone the absence of visible vortices in recent experiments [14]. An explanation derived in Refs. [14,16] to account for the lack of visibility of vortices is that a small fraction of the gas is at higher temperature and thus decreases the visibility of vortices. The vortex lattice should be visible only at ultralow temperature that cannot be reached in the experiments. Our study seems to favor this hypothesis: when looking for the ground state of the system, we found that much longer times were required for large Ω to reach a well-ordered vortex lattice [the convergence time to reach a stable state in Figs. 3(c) and 3(d) is 3–4 times larger than for Fig. 3(a)]. Transient states before convergence (which seems to correspond to experimental observations) display incomplete vortex reconnection and an irregular lattice structure. This confirms the hypothesis of the fragility of the vortex lattice in the regime of fast rotation.

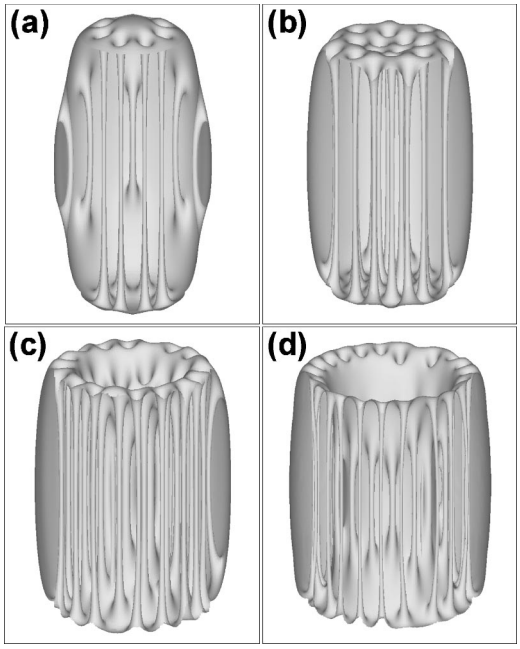

FIG. 4. ($\alpha=0.9$) Side view of the condensate for $\Omega/\omega_\perp=0.32$ (a), 0.4 (b), 0.48 (c), and 0.56 (d).

For $\Omega/\omega_\perp=0.56$ [Figs. 3(d) and 4(d)], the central vortices have completely merged into a giant vortex. The lattice still exist around as two concentric rings of singly quantized vortices.

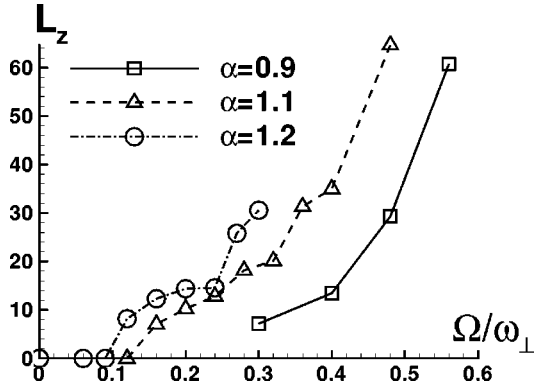

FIG. 5. Angular momentum L_z (in units of $\hbar$) for all studied configurations.

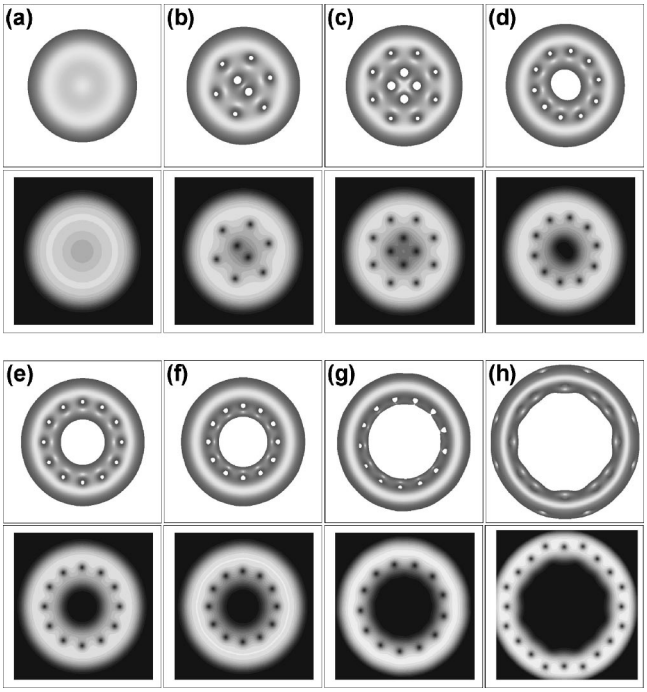

FIG. 6. ($\alpha=1.1$) Top view of the isosurface of lowest density (up) and density contours in the plane $z=0$ (down) for $\Omega/\omega_\perp=0.12$ (a), 0.16 (b), 0.2 (c), 0.24 (d), 0.28 (e), 0.32 (f), 0.4 (g), and 0.48 (h).

Increasing $\Omega/\omega_\perp$ to 0.64 leads to a larger central hole surrounded by a single ring of vortices (pictures not shown), and a large value of the angular momentum ($L_z\approx 100$). It would be an interesting theoretical problem to understand the criterion for the existence of a single ring of vortices around the hole. This should depend on the size of the condensate, the size of the annulus and on Ω.

B. Intermediate repulsive case ($\alpha=1.1$)

Since the regime of fast rotation is experimentally difficult to investigate, we suggest in the following section a new form of trapping potential that allows to obtain giant vortices for lower rotation frequencies and with smaller time of stabilization, leading to less fragile vortices.

The trapping potential (7) for this case has a *quartic–minus-harmonic* form and displays a Mexican hat shape (Fig. 1). The shapes of the solutions are plotted in Figs. 6 (top view and $z=0$ cuts) and Figs. 7 (side view).

The transition from isolated vortices to a hole with a circle of singly quantized vortices around is observed. This happens for lower rotation frequencies and with a smaller number of vortices than in the previous case, that is, before a dense lattice is formed. For Ω small, the density of the solution has a depletion close to the center but no hole and no vortices are observed [Figs. 6(a) and 7(a)]. For Ω larger [Fig. 6(b)], vortices are nucleated and the angular momentum L_z starts to grow (Fig. 5).

For $0.16\leqslant\Omega/\omega_\perp<0.24$, the density of the solution is zero close to the top and bottom of the condensate, but not at the center, which gives rise to a special structure of vortices

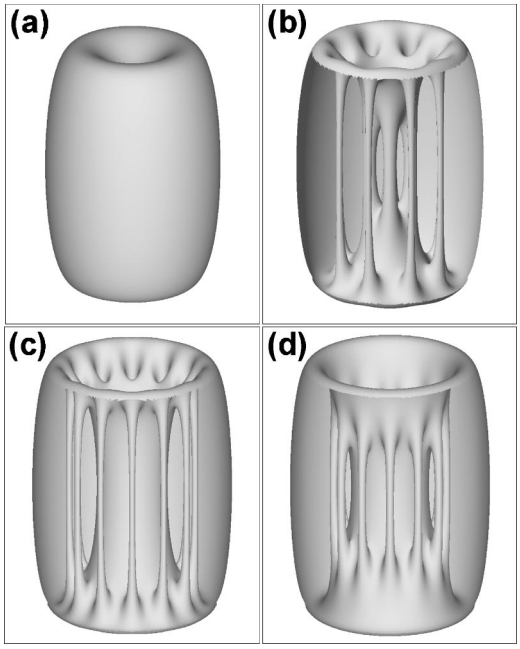

FIG. 7. ($\alpha=1.1$) Side view of the condensate for $\Omega/\omega_\perp=0.12$ (a), 0.2 (b), 0.28 (c), 0.32 (d). Isosurface of lowest density.

[Fig. 7(b)]: the top view [Fig. 6(b) and 6(c)] indicates that vortices arrange themselves along two concentric circles. The inner circle is made up of vortices which are isolated in the center of the condensate but reconnect towards the top of the condensate to form a giant vortex [Fig. 7(b)]. The outer circle is made up of almost straight *U* vortices that reconnect to the top and bottom of the condensate. As Ω increases, the number of vortices on each circle increases. In Figs. 6(b) and 6(c), the inner vortices seem to be bigger, but this is just an effect due to the projection and the bending: the view at $z=0$ allows to check that all vortices have the same size.

For $\Omega/\omega_\perp=0.24$ [Figs. 6(d) and 7(c)], the straight vortices that were close to the axis of the condensate have merged into a central hole. There are also isolated vortices regularly scattered on a circle around the giant vortex. As Ω increases, the number of vortices inside and outside the giant vortex increases and the length of the isolated vortices decreases as can be seen in Figs. 7(c) and 7(d).

Note that the isolated vortices are *U* vortices that reconnect to the giant vortex at the center, not to the boundary of the condensate, as in the case of the harmonic trapping [15], that is, their bending is concave not convex.

For $\Omega/\omega_\perp=0.48$ [Figs. 6(h) and 8], the number of vortices has increased. On the top view [Fig. 6(h)], there seems to be two outer circles of vortices around the giant vortex, whereas the view at $z=0$ indicates that there is only one: the inner *U* vortices reconnect to the giant vortex and the outer to the outer boundary of the condensate. Both have different concavity in their bending as illustrated in Fig. 8. This may be explained using the analysis of Refs. [17,18]: the bending of the vortex depends on its location with respect to the level lines $\rho_{\mathrm{TF}}=cst$. The vortex is almost straight in its central part and then reaches the boundary using the shortest distance: for harmonic trapping and oblate condensates, it leads to U vortices, for harmonic trapping and prolate condensates, it

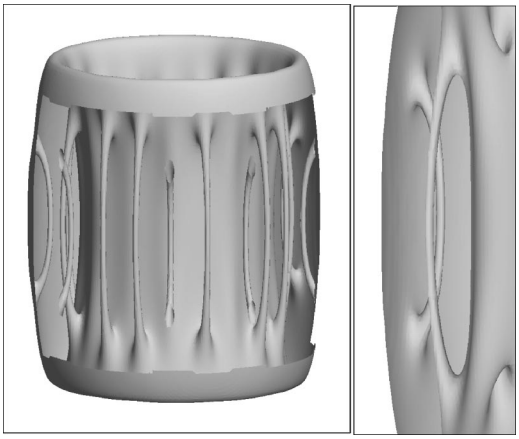

FIG. 8. ($\alpha=1.1$) Vortex details for $\Omega/\omega_\perp=0.48$.

leads to straight vortices and in this case, it should lead to a bending direction depending on the location of the straight part of the vortex; namely, if we plot the line equidistant to the inner and outer boundary of the condensate with respect to the distance $\int_\gamma \rho_{\mathrm{TF}}\, dl$, then this divides the condensate into two regions, one where vortices bend inwards and the other where they bend outwards.

These simulations open a few interesting directions of theoretical work: understand why the merging of the lattice starts from the top of the condensate to the center, and how the length of vortices decreases with Ω. Let us point out that the transition from vortex lattice to giant vortex has been analyzed in 2D [10]. But this analysis requires a large number of vortices. With the type of trapping potential that we have studied, the number of vortices at the transition is low, and we believe that the analytical tools to be developped should be different from the ones used up to now.

C. Strong repulsive case ($\alpha=1.2$)

In this case, the effective potential has a Mexican hat structure for all Ω and the density profile of the solution always has a hole in the center as illustrated in Fig. 9. For low values of Ω, the density has a dip, without circulation, there are no vortices, that is $L_z=0$ (Fig. 5); it is only the modulus of the solution that goes to zero. For $\Omega/\omega_\perp \geqslant 0.12$, the hole contains a giant vortex and L_z increases with Ω (see Fig. 9).

The giant vortex phase profiles (Fig. 10), which are similar to those obtained in the 2D simulations [12], show that the phase singularities do not completely overlap in the center of the vortex. Consequently, the giant vortex can be regarded as a hole containing singly quantized vortices with such low density that they are discernible only by the phase defects. Let us point out that the plot in Fig. 10 only takes into account the vortices inside the hole.

As Ω is increased, there is a giant vortex which turns into a giant vortex with a single circle of vortices around. In the previous cases, this type of transition did not take place as Ω was increased but decreased. It is characterized by a dramatic increase of the angular momentum L_z (Fig. 5). To our knowledge, this transition (which is similar to the case of the rotating bucket experiment for helium) has not been studied in BEC. It would be interesting to predict the location of the isolated vortices around the giant vortex and their height. For the moment, we have a work in progress [19] in the spirit of Ref. [17] to characterize in this setting the location of the circle of vortices in terms of ρ_{TF}. The 3D equivalent requires more tools.

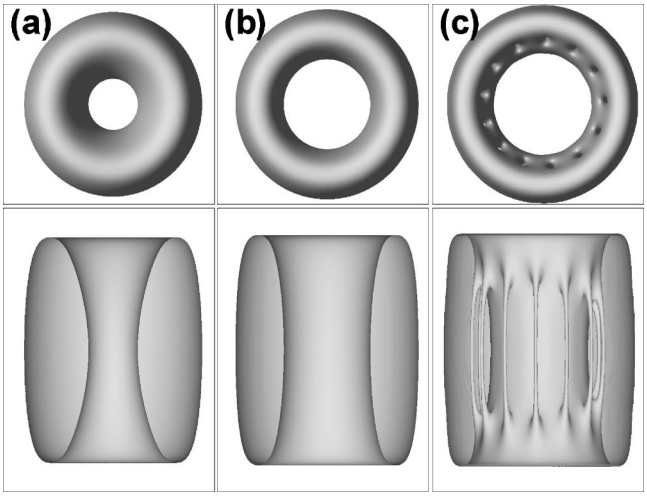

FIG. 9. ($\alpha=1.2$) Top and side view of the condensate for $\Omega/\omega_\perp=0.12$ (a), 0.2 (b), and 0.3 (c).

A question raised by A. L. Fetter [20] is whether increasing Ω further would lead to a disappearance of the circle of vortices around the giant vortex. The angular velocity required seems to be beyond our computational possibilities since the size of the annulus has to get of the order of the mesh.

IV. CONCLUSION

We have studied stable configurations of the Gross Pitaveskii energy when the trapping potential has a combined quartic and harmonic term.

For weak quartic potentials, the solution evolves from a vortex lattice to a vortex array with hole when the angular velocity Ω is increased. For stronger quartic potentials, giant vortices are obtained for lower Ω, at a stage where the lattice

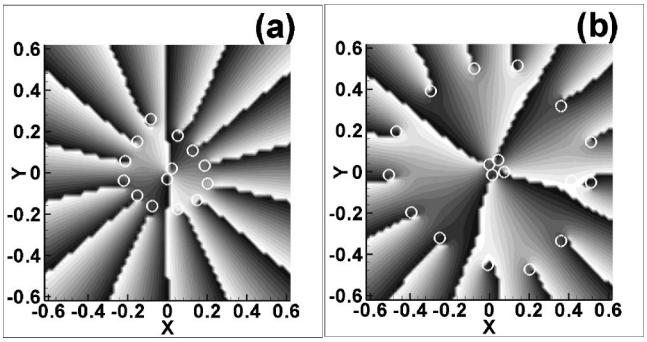

FIG. 10. ($\alpha=1.2$) Phase distribution in a central $z=0$ cut plane. $\Omega/\omega_\perp=0.2$ (a) and 0.3 (b). Open circles mark phase defects located inside the central hole seen in Fig. 9.

is not so dense. The typical structure of vortices has a central giant vortex with an outer circle of vortices around. We believe that there should be a criterion depending on the radius of the condensate and the radius of the annulus that should characterize the final structure of the giant vortex: whether there is or not a circle of vortices around the giant vortex and its precise location.

In the regime of fast rotation, the 2D picture seems to be a good approximation since vortices are almost straight. We show more details on the three-dimensional structure of vortices and understand the 3D effects of the trapping potential on the number, shape, and location of vortices, as Ω is increased. The merging process of individual vortices into a giant vortex is shown to be highly three dimensional.

The form of the potential considered in our simulations was inspired from recent experiments [13]. The regime of fast rotation leads to a fragile lattice which needs long time to stabilize. We have checked that keeping the exponential part of the potential instead of its *quartic minus harmonic* approximation does not change the qualitative behavior of the solutions. This suggests that if this situation could be achieved experimentally, it would allow to observe giant vortices for lower velocities than previously, that is, before reaching the fast rotation regime.

ACKNOWLEDGMENTS

We would like to acknowledge stimulating discussions with V. Bretin and J. Dalibard

[1] M. R. Matthews *et al.*, Phys. Rev. Lett. **83**, 2498 (1999).
[2] K. Madison, F. Chevy, V. Bretin, and J. Dalibard, Phys. Rev. Lett. **84**, 806 (2000).
[3] K. Madison, F. Chevy, W. Wohlleben, and J. Dalibard, J. Mod. Opt. **47**, 2715 (2000).
[4] C. Raman, J. R. Abo-Shaeer, J. M. Vogels, K. Xu, and W. Ketterle, Phys. Rev. Lett. **87**, 210402 (2001).
[5] K. W. Madison, F. Chevy, V. Bretin, and J. Dalibard, Phys. Rev. Lett. **86**, 4443 (2001).
[6] J. R. Abo-Shaeer, C. Raman, J. M. Vogels, and W. Ketterle, Science **292**, 476 (2001).
[7] P. Rosenbusch, V. Bretin, and J. Dalibard, Phys. Rev. Lett. **89**, 200403 (2002).
[8] A. L. Fetter, Phys. Rev. A **64**, 063608 (2001).
[9] E. Lundh, Phys. Rev. A **65**, 043604 (2002).
[10] G. M. Kavoulakis and G. Baym, New J. Phys. **5**, 51.1 (2003).
[11] U. R. Fischer and G. Baym, Phys. Rev. Lett. **90**, 140402 (2003).
[12] K. Kasamatsu, M. Tsubota, and M. Ueda, Phys. Rev. A **66**, 053606 (2002).
[13] V. Bretin, S. Stock, Y. Seurin, and J. Dalibard, Phys. Rev. Lett. **92**, 050403 (2004).
[14] S. Stock, V. Bretin, S. Stock, F. Chevy, and J. Dalibard, e-print cond-mat/0311099.
[15] A. Aftalion and I. Danaila, Phys. Rev. A **68**, 023603 (2003).
[16] J. Dalibard (private communication).
[17] A. Aftalion and T. Riviere, Phys. Rev. A **64**, 043611 (2001).
[18] A. Aftalion and R. L. Jerrard, Phys. Rev. A **66**, 023611 (2002).
[19] A. Aftalion, L. Bronsard, and S. Alama (unpublished).
[20] A. L. Fetter (private communication).